Microchimica Acta (2020) 187: 608
https://doi.org/10.1007/s00604-020-04586-z

ORIGINAL PAPER

Environmental and intercellular Pb^{2+} ions determination based on encapsulated DNAzyme in nanoscale metal-organic frameworks

Weihao Wu[1] · Yaofang Fan[1] · Bing Tan[1,2] · Huimin Zhao[1]

Received: 20 February 2020 / Accepted: 1 October 2020 / Published online: 14 October 2020

Abstract

With the merits of low cost, simple synthesis procedure, and high affinity for metal ions, deoxyribozyme (DNAzyme) have played important roles in metal ions detection. However, the intracellular applications of DNAzyme are limited because of enzymatic degradation and inefficient cellular uptake. To address these problems, GR-5 as model DNAzyme was encapsulated into zeolitic imidazolate frameworks-8 (ZIF-8) nanoparticles by biomimetic mineralization. The positively charged ZIF-8 with high DNAzyme loading capacity retained their ability to enter cells. Compared with free DNAzyme, the biomimetic mineralization synthesis method has greatly improved the stability of pristine DNAzyme. The as-synthesized DNAzyme@ZIF-8 composite exhibited good stability resisting DNase I, and was used as a sensitive fluorescent nanoprobe for Pb^{2+} determination and successfully achieved selective and sensitive determination for Pb^{2+} at $\lambda_{ex}/\lambda_{em}$ = 494/522 nm in real samples. The linear range for the determination of Pb^{2+} is 50 to 500 nM. Moreover, the highly active DNAzyme delivered by ZIF-8 allows noninvasive imaging of Pb^{2+} measurement in living cells. This strategy will extend the suitability of functional nucleic acids for in vitro and in vivo bioanalysis and bioimaging.

Keywords DNAzyme · Metal-organic frameworks · Biomimetic mineralization · Lead detection · Fluorescence

Introduction

In 1994, a RNA-cleaving DNA enzyme (DNAzyme) was firstly reported for catalyzing the Pb^{2+}-dependent cleavage of an RNA phosphoester through in vitro selection methods [1]. In the presence of Pb^{2+}, the enzyme strand can cleave the RNA linkage (rA) in the substrate strand. Generally, the DNAzyme is formed by a substrate strand and an enzyme strand. The substrate strand contains a single rA that serves as a cleavage site while the enzyme strand consists of one catalytic core and two binding arms [2]. Up to now, various DNAzymes have been isolated to catalyze many chemical reactions, including RNA cleavage [3–6], DNA cleavage [7, 8], DNA/RNA ligation [9–11], and DNA phosphorylation reactions [12]. Due to the specifically dependent on cofactors and multiple enzymatic turnover properties, DNAzyme have been widely utilized for constructing various metal ions responsive biosensors [13, 14]. For cofactors of Pb^{2+}, DNAzymes possess high binding affinities and selectivities. Compare to protein enzymes, DNAzymes possess better stability and cost less to produce [15, 16]. The above features make DNAzymes particularly attractive for constructing Pb^{2+} biosensor platform.

Metal ions play important roles in kinds of biological processes. DNAzyme-based platforms showed great promise for metal ions detection inside cells [17]. However, the inefficient cellular uptake and enzymatic degradation limit the biological applications of DNAzyme [18]. Thus, developing an effective method to achieve efficiently cellular uptake and enhance stability is necessary for improving DNAzyme in cellular detecting application.

Weihao Wu and Yaofang Fan contributed equally to this work.

Electronic supplementary material The online version of this article (https://doi.org/10.1007/s00604-020-04586-z) contains supplementary material, which is available to authorized users.

✉ Huimin Zhao
zhaohuim@dlut.edu.cn

[1] Key Laboratory of Industrial Ecology and Environmental Engineering (Ministry of Education, China), School of Environmental Science and Technology, Dalian University of Technology, Dalian 116024, China

[2] School of Environment, Key Laboratory for Yellow River and Huai River Water Environment and Pollution Control, Ministry of Education, Henan Normal University, Xinxiang 453007, China

Recently, biomimetic nanomaterials were developed to simulate function of natural substances [19, 20]. Metal-organic frameworks (MOFs), which are constructed with metal ions or clusters and organic ligands by coordination bonds [21], have been proved to be a potential platform in biological applications [22]. In particular, MOFs have also been gradually explored for the immobilization of biomolecules. Various biomolecules, such as enzymes [23], drugs [24], and DNA [25], have been successfully immobilized on MOFs. Since the first report in 2006 [26], the number of studies regarding the immobilization of enzymes on MOFs has increased rapidly [27–29]. Zeolite imidazole frameworks-8 (ZIF-8), as a kind of typical porous materials, which is consist of zinc ions and 2-methylimidazole (2-MIM) by coordination bonds. ZIF-8 not only exhibits features of large porosity and surface area as MOFs but also possesses other advantages including exceptional thermal and chemical stability, low cost and easy synthesis, which performed as an ideal material for enzyme immobilization [30–32]. Liang et al. demonstrated the first example of embedding horseradish peroxidase into ZIF-8, which enhanced the enzyme stability of resisting extreme conditions such as high temperature and organic solvents [23]. Ge et al. also presented a method for immobilizing glucose oxidase (GOx) and horseradish peroxidase (HRP) into ZIF-8 by co-precipitation, which enhanced the thermal stability and resistance to proteolysis of enzymes [33]. Guo et al. developed the DNA@ZIF-8 hybrid membrane into direct methanol fuel cells. The selectivity of the DNA@ZIF-8 membrane is thus significantly higher than that of developed proton-exchange membranes for fuel cells [34].

Up to now, most researches on MOF/enzyme composites have been mainly focused on immobilization of enzymes and proteins. Several pioneering studies reported that ZIF-8 can achieve the tumor-targeting accumulation of DNA payloads and can facilitate the subsequent cellular uptake of DNA without degradation [35, 36]. Immobilization of DNA in biological applications is still in the preliminary stage. A detailed understanding of how ZIF-8 encapsulates DNA will expand the use of MOFs in biosensor and biotechnology. We anticipated that the ZIF-8-encapsulating DNAzyme nanoplatform could be developed as a smart theranostic system with substantially enhanced stability for Pb^{2+} determination.

Herein, we report the synthesized, characterization and catalytic activity of ZIF-8@DNAzyme composite by biomimetic mineralization. Our ZIF-8 nanospheres have uniform 140 nm size, which is optimal for cellular uptake and stable under aqueous physiological conditions. DNAzyme loading is achieved under mild conditions. GR-5 as model DNAzyme encapsulated into ZIF-8 via biomimetic mineralization was involved in the fluorescent assay. The stability of the crystalline composites was discussed via enzyme digestion reaction.

As shown in scheme 1, the DNAzyme of Pb-Sub strand was attached with a fluorophore (FAM) at the 5′ end, and the Pb-Enz strand was labeled with a quenching probe (BHQ) at the 3′ end. The DNAzyme strand and the substrate strand first formed a stable DNAzyme–substrate duplex probe. The fluorescence resonance energy transfer (FRET) will occur between fluorophore FAM and BHQ. The presence of target metal ions Pb^{2+}, Pb^{2+} as assistors trigger DNAzyme cleavage processes and then induce the release of the fluorophore-labeled DNA fragment, achieving the restoration of the fluorescence signal. Subsequently, the DNAzyme–substrate duplex probe was encapsulated of DNAzyme into ZIF-8 through biomimetic mineralization. A unique nanoplatform was constructed and successfully achieved the determination of lead ions in real samples.

Experimental section

Materials and reagents

The nucleic acids Pb-Enz (5'-ACAGACATCATCTC TGAAGTAGCGCCGCCGT ATAGTGAG-BHQ-1-3′) and Pb-Sub (5'-FAM-CTCACTAT/rA/GGAAGAGATGAT GTCTGT-3′) were synthesized by Sangon Biological Engineering Technology & Company Ltd. (Shanghai, China) and purified by high-performance liquid chromatography (HPLC).NaCl, $MgCl_2$, $CuCl_2$, $Pb(NO_3)_2$, $Zn(NO_3)_2$, $BaCl_2$, and $MnCl_2$ were of analytical reagent grade and purchased from the Sinopharm Chemical Reagent Co., Ltd. (Shanghai, China). 2-methylimidazole ($C_4H_6N_2$, 99%) were obtained from Aladdin Reagent Co., Ltd. (Shanghai, China). Ultrapure water obtained from a Millipore water purification system (resistivity > 18.0 ΩM cm^{-1}, Laikie Instrument Co., Ltd., Shanghai, China) was used throughout. All other reagents were of analytical grade.

Instruments

FL measurements were performed using Hitachi F-4500 fluorescence spectrometer with a scan rate at 1200 nm/min. The excitation wavelength was set at 494 nm. The excitation and emission slit were set at 5 nm/10 nm with a 700 V photomultiplier tube (PMT) voltage. SEM images were conducted by a Hitachi S-4800 scanning electron microscopy. X-ray measurements were collected on a LabX XRD-7000 X-ray diffractometer (XRD). Brunauer–Emmett–Teller (BET) was used to determine the surface area and pore size distribution. Zeta potential measurements were carried out using a Zetasizer Nano ZS90 (Malvern, ZEN3690).

Synthesis of DNAzyme/ZIF-8 composite

A 0.28 g of 2-methylimidazole was dissolved in 1 mL ultrapure water. Fifteen milligram of $Zn(NO_3)_2{\cdot}6H_2O$ was

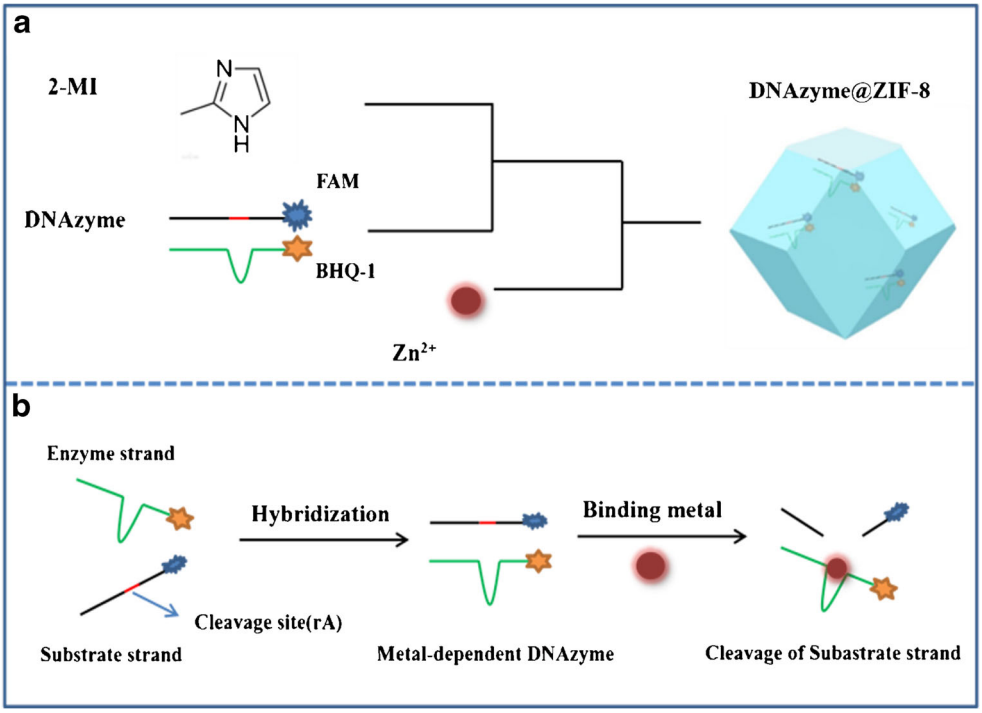

Scheme 1 **a** Schematic illustration of the synthesis of DNAzyme@ZIF-8 composite. **b** Working principle of DNAzyme for metal ions fluorescent detection

dissolved in 0.1 mL ultrapure water. The solution of $Zn(NO_3)_2{\cdot}6H_2O$ was added into the solution of 2-methylimidazole under stirring. After incubating for 2 h, 100 μL of DNAzyme (25 μM) was added into the aqueous mixture of 2-methylimidazole and $Zn(NO_3)_2{\cdot}6H_2O$ under stirring. After reacting for 2 h, the product was collected by centrifugation at 6500 r.p.m. for 10 min. Afterward, the obtained precipitate was sonicated and centrifuged thrice in water followed by ethanol. Part of the product was used for characterizations by lyophilization.

Synthesis of DNAzyme@ZIF-8 composite

According to the previous method with some adjustment, the DNAzyme@ZIF-8 composite was synthesized [23]. A 0.28 g of 2-methylimidazole and 100 μL of DNAzyme (25 μM) were dissolved in 1 mL ultrapure water. Fifteen milligrams of $Zn(NO_3)_2{\cdot}6H_2O$ was dissolved in 0.1 mL ultrapure water. The solution of $Zn(NO_3)_2{\cdot}6H_2O$ was added into the aqueous mixture of 2-methylimidazole and DNAzyme under stirring. After incubating for 2 h, the product was collected by centrifugation at 6500 r.p.m. for 10 min. Afterward, the obtained precipitate was sonicated and centrifuged thrice each in water followed by ethanol. Part of the product was used for characterizations by lyophilization.

FL assay of Pb^{2+}

In a typical experiment, 200 nM DNAzyme modified ZIF-8 was added to 50 mM N-2-hydroxyethylpiperazine-N-ethanesulphonicacid (HEPES) buffer (50 mM NaCl, 5 mM $MgCl_2$, pH 7.26), then a certain concentration of Pb^{2+} was added to the above-mixed solution and incubated at 37 °C for 4 h. Finally, at room temperature, the fluorescent spectrum of the mixture was recorded by F-4500 fluorescence spectrometer at $\lambda_{ex}/\lambda_{em}$ = 494/522 nm.

ICP assay of Pb^{2+}

In a typical experiment, 200 nM DNAzyme modified ZIF-8 was added to 50 mM N-2-hydroxyethylpiperazine-N-ethanesulphonicacid (HEPES) buffer (50 mM NaCl, 5 mM $MgCl_2$, pH 7.26), then 200 nM Pb^{2+} was added to the above-mixed solution and incubated at 37 °C for 4 h. The product was collected by centrifugation at 6500 r.p.m. for 10 min to wash away the unbound Pb^{2+}. The washed collection was digested for 1 h with 3 mL concentrated nitric acid and 1 mL concentrated sulfuric acid. Then, the digested solution was appropriately diluted and determined by ICP.

Imaging analysis in cells

Two hundred ninety-three T cells and Huh-7 cells were respectively dispersed in a 24-well microtiter plate with 1.0×10^3 and 1.0×10^4 cells per well. Lead ion was first added to the above two types of cells. After incubating for 4 h, the cells were washed three times with 0.1 mM PBS buffer. Afterward, the DNAzyme@ZIF-8 composite was added into the two Pb-incubated cells and incubated for 4 h and 24 h. The

fluorescence images were obtained by using a confocal laser scanning fluorescence microscope (CLSM).

Results and discussion

Characterization of DNAzyme@ZIF-8 composite

Encapsulation of DNAzyme into ZIF-8 was first confirmed by confocal microscopy using FAM-DNAzyme@ZIF-8. The DNAzyme in FAM-DNAzyme@ZIF-8 was also composed of two chains. Only the FAM is labeled in the substrate chain, while the quencher group is not labeled in the enzyme chain. As shown in Fig. 1a, FAM-DNAzyme@ZIF-8 composites that were only labeled with FAM were prepared and the fluorescence signal of FAM-DNAzyme@ZIF-8 was observed through confocal laser scanning fluorescence microscopy, which demonstrated the encapsulation of DNAzyme. The tunable pore size and rigid molecular structure of ZIF-8 allow the encapsulation of nucleic acids stability under harsh conditions [37]. Moreover, nanoscale MOFs can be efficiently internalized by cells for intracellular delivery [38]. Because of the positive charged Zn^{2+} on the surface of ZIF-8, ZIF-8 as a nanocarrier can efficiently deliver a nucleic acid probe to living cells [39]. And the morphology and size of the ZIF-8 and DNAzyme@ZIF-8 composite were inspected by SEM. The ZIF-8 particles were nanocrystals with polyhedral shape and the size was approximately 140 nm (Fig. S1).

Fig. S2 showed the SEM image of DNAzyme@ZIF-8, which displayed similar size and shape to ZIF-8, indicating that the encapsulation of DNAzyme did not affect the morphology of ZIF-8. Then, powder XRD was further used to confirm the construction of the synthesized ZIF-8 and DNAzyme@ZIF-8. Compared with the simulated XRD pattern, no impurity peaks could be found in the XRD pattern of synthesized ZIF-8, suggesting synthesized ZIF-8 was well crystallized. And the XRD pattern of DNAzyme@ZIF-8 composite indicated that the encapsulation of the DNAzyme did not affect the crystal structure of ZIF-8 (Fig. 1b). As revealed in Fig. 1c and d, both the N_2 adsorption measurement of ZIF-8 and DNAzyme@ZIF-8 composite showed type I isotherms characteristics of mesopores. Compared to ZIF-8, DNAzyme@ZIF-8 composite showed a slight increase in hysteresis at higher p/p_0 ratio indicating presence of few mesopores along with micropores. Then, the zeta potential was measured. ZIF-8 nanoparticles showed positive zeta potential, which might be attributed to abundant positively charged Zn^{2+} on the surface of ZIF-8 [39]. Zeta potential of DNAzyme/ZIF-8 composite more decreased than that of ZIF-8, strongly demonstrating the adsorption of the DNAzyme on the surface of ZIF-8 through electrostatic interaction (Fig. S3). While DNAzyme@ZIF-8 composite showed similar zeta potential to ZIF-8, it strongly demonstrated the encapsulation of DNAzyme

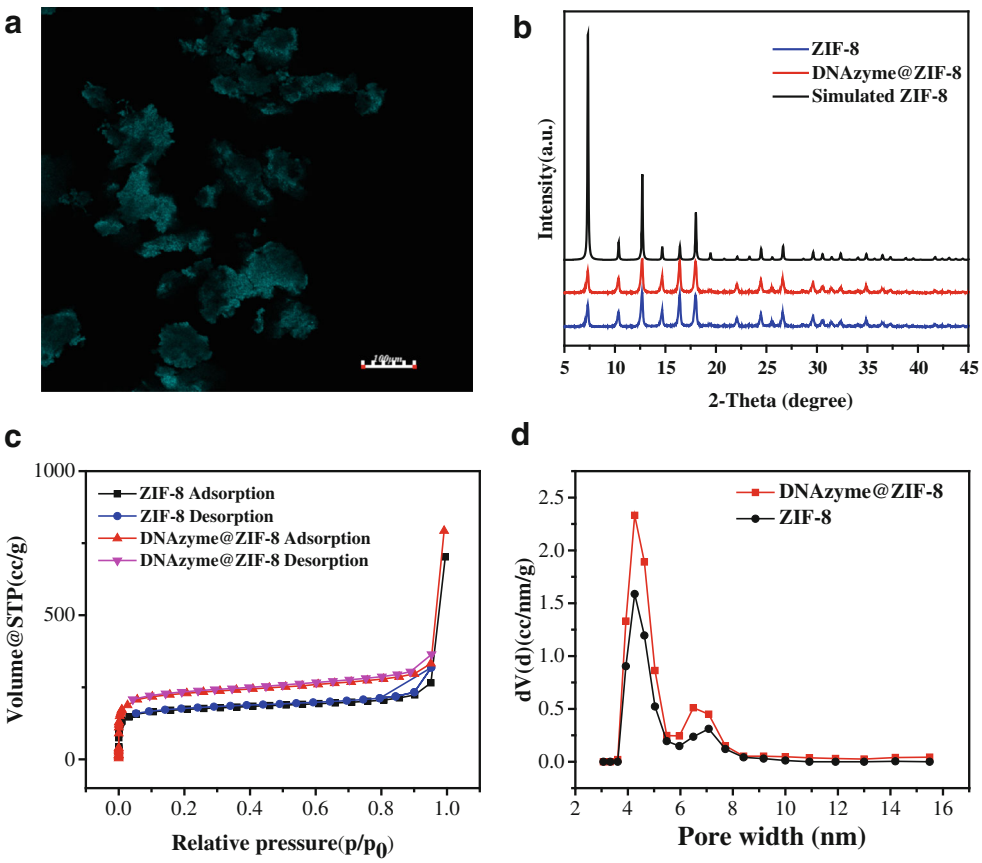

Fig. 1 **a** Confocal microscopy image of the FAM-DNAzyme@ZIF-8 composite, the scale bar is 100 μm. **b** XRD patterns of pure ZIF-8 (blue), DNAzyme@ZIF-8 composite (red), and simulated ZIF-8 (black). **c** Nitrogen sorption isotherms of ZIF-8 and DNAzyme@ZIF-8. **d** Pore size distributions of ZIF-8 and DNAzyme@ZIF-8

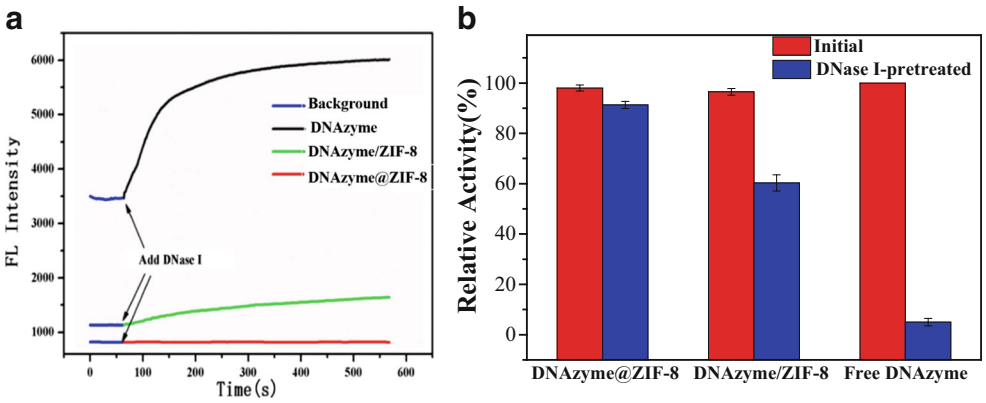

Fig. 2 **a** Fluorescence changes with time of the free DNAzyme (black), DNAzyme/ZIF-8 (green), and DNAzyme@ZIF-8 (red) after adding DNase I. **b** Comparison of the initial activity of the DNAzyme@ZIF-8, DNAzyme/ZIF-8 and free DNAzyme, and the activity after addition of DNase I

into ZIF-8 successfully by biomimetic mineralization. The DNAzyme loading capacity was quantitatively measured by examining the fluorescence intensity of the FAM-labeled DNAzyme in the precursor solution and in the supernatant of the acquired product. According to the pre-determined calibration curve, the loading capacity of DNAzyme@ZIF-8 was confirmed to be as high as 95.2 ± 2.2%, which was higher than the loading capacity of DNAzyme/ZIF-8 (Fig. S4).

Optimization of method

An increase of the ratio between Zn^{2+} and 2-MI resulted in the decrease of the size of ZIF-8 (Fig. S5) and the loading capacity of DNAzyme (Fig. S6). Although the loading capacity at the ratio of 1:35 is higher than that at the ratio of 1:70, oversized ZIF-8 would hinder the accessibility into cell. The results of SEM-EDS were shown in Fig. S7. Compared to ZIF-8, Zn, C, and N are dispersed over DNAzyme@ZIF-8 revealing ZIF-8 existence. O an P elements reveal the composite of DNAzyme over the DNAzyme@ZIF-8. According to the pre-determined calibration curve, the loading capacity of DNAzyme was measured. With the range from 10 to 10 μM, ZIF-8 exhibited high DNAzyme loading capacity (Fig. S8). Next, 200 nM Pb^{2+} was incubated with DNAzyme@ZIF-8 composite and ZIF-8, respectively. After incubation, the concentration of Pb^{2+} in DNAzyme@ZIF-8 composite and ZIF-8 was determined 23.25 μg/L (111.77 nM) and 0.16 (0.76 nM) by ICP-MS, indicating that Pb^{2+} loaded of DNAzyme. The ratio between Pb-Enz and Pb-Sub was optimized to obtain the best detection performance. With the decrease of the radio between Pb-Enz and Pb-Sub (2:1, 3:2, 1:1), an increase of $(F\text{-}F_0)/F_0$ was observed (Fig. S9). However, further reducing Pb-Enz affected the performance of nanoprobe due to the high background signal. On basis of this result, Pb-DNAzyme with the 1:1 Pb-Enz and Pb-Sub ratio and ZIF-8 with the 1:70 Zn^{2+} and 2-MI was selected for the following experiments.

Stability of nanoprobe

Here, the stability of the DNAzyme@ZIF-8 composite against DNase I as the model digesting enzyme was examined. As shown in Fig. 2a, in the absence of DNase I, the free DNAzyme and DNAzyme@ZIF-8 maintained stable fluorescence intensity. While DNase I was added, the fluorescence of DNAzyme@ZIF-8 was unchanged, which indicated that ZIF-8 acted as a protective layer for DNAzyme, protecting DNAzyme from DNase I degradation. On the contrary, the fluorescence of the double-stranded formed by FAM-labeled substrate strands and BHQ-1-labeled enzyme strands increased quickly after adding DNase I, which demonstrated that free DNAzyme was easily degraded by DNase I, the FAM was no longer quenched by BHQ-1, resulting in the recovery of fluorescence. In these biocomposites, the ZIF-8 shell was shown to protect DNAzyme from cell environments that typically lead to their degradation, acting as a gate for molecular transport. Partial fluorescence recovery was observed in DNAzyme/ZIF-8, indicating that adsorption possessed a weaker protective effect on DNAzyme compared with biomimetic mineralization. It may due to enzymes are physically absorbed onto the ZIF-8 surface through weak interactions, which often results in enzyme leakage [40]. As revealed in Fig. 2b, after incubating with DNase I for 10 min, compared to the initial activity, free DNAzyme lost nearly all its activity. DNAzyme/ZIF-8 exhibited certain resistibility but also lost partial activity. However, DNAzyme@ZIF-8 composite kept almost the same activity after the same treatment, proving an excellent resistivity against DNase I.

Detection for Pb^{2+}

In a typical experiment, the time-dependent fluorescence changes at 522 nm were measured after the addition of a certain concentration of Pb^{2+}. The calibration curve for the assay was shown in Fig. 3a, as the Pb^{2+} ions concentration ranged from 0 to 5 μM, the increase of the fluorescence

Table 1 Analytical features based on DNAzyme for Pb^{2+} detection in water

Technique	Strategy	Detection range (nM)	LOD (nM)	Ref.
FRET	GO-DNAzyme–based biosensor for amplified fluorescence	1–100	0.3	[42]
FRET	Pb^{2+}-dependent DNAzyme–based evanescent wave-induced emission	20–800	1	[43]
UV-vis	AuNP-based label-free colorimetric method using DNAzyme	0.5–5	0.2	[44]
FRET	17E DNAzyme and the cleavage substrate 17S labeled with FAM	0–100	0.53	[45]
FRET	Dual-emission DNA templated silver nanoclusters	0.001–10	0.001	[46]
FRET	DNAzyme@ZIF-8	50–500	39	This work

intensity was observed, indicating that more and more FAM-labeled substrate strands were cleaved and released from the ZIF-8 with the increasing Pb^{2+} concentration. In the absence of Pb^{2+}, no fluorescence enhancement was observed in the controlled experiment. The original concentration of the Pb^{2+} was chosen between 0 to 5.55 μM. After the sample being diluted for 1.11 times, the detection range of the final concentration of Pb^{2+} was between 0 to 5 μM. With the concentration of Pb^{2+} ranging from 50 to 500 nM, the proposed method exhibited a linear relationship $Y = 0.06X + 66.90$ (Y stands for FL intensity, X stands for Pb^{2+} concentration (nM)) with a good linear response ($R^2 = 0.996$) of fluorescence intensity (Fig. 3a). The detection limit of Pb^{2+} was estimated to be 39 nM based on the 3δ/slope rule, which was lower than 72 nM, the safety limit of lead in drinking water (72 nM) defined by the United States Environmental Protection Agency (EPA). After compared with other reported Pb^{2+} detection methods based on DNAzyme in water (Table 1), it is found that the proposed fluorescent method shows comparable analytical performances including wide linear range and high sensitivity. Particularly, ZIF-8 as a nanocarrier could protect DNAzyme from DNase degradation. In addition, DNAzyme@ZIF-8 composite with the positively charged Zn^{2+} on the surface makes easily to adsorb at the negatively charged cell membrane to efficiently deliver DNAzyme into living cells for imaging. Besides sensitivity, selectivity was another important issue to assess the detection performance of this newly proposed nanoprobe. The GR-5 has been reported with high selectivity to Pb^{2+} [41]. To confirm the selectivity of the system, the responses of the system in potentially interfering metal ions were measured, including

Table 2 The determination of Pb^{2+} in tap water samples

Sample	Add/nM	Found/nM	Recovery/%	ICP-MS/nM
Tap water (1)	0	16.63		0
Tap water (2)	100	128.10	111.4	102.93
Tap water (3)	250	248.05	92.5	275.58
Tap water (4)	500	518.28	100.3	576.67

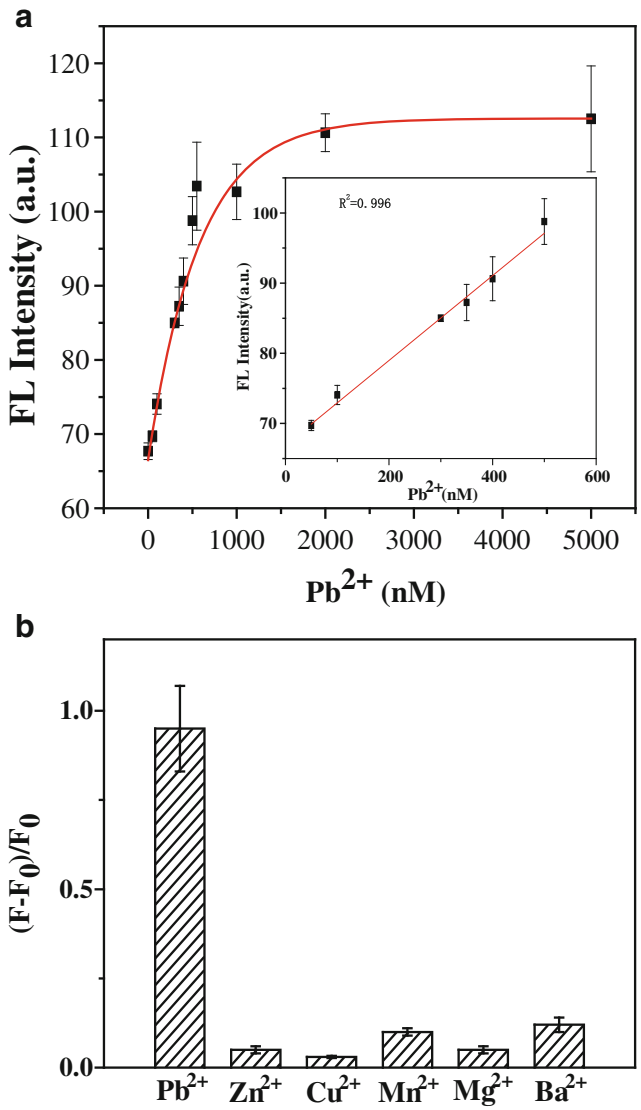

Fig. 3 **a** Calibration curve of the method for Pb^{2+}. The curve was plotted with the fluorescence change as Pb^{2+} concentration (0–5 μM). Insert: the linear relationship between the fluorescence intensity and concentrations of Pb^{2+} from 50 to 500 nM. **b** The selectivity of the method for Pb^{2+} detection over other competitive metal ions. The concentration of Pb^{2+} and other metal ions was set at 1 μM and 100 μM, respectively. The buffer contained 50 mM HEPES (pH 7.26), 50 mM NaCl and 5 mM $MgCl_2$. Fluorescence was measured at 522 nm. Error bars represent the standard deviation in three individual experiments

Zn^{2+}, Cu^{2+}, Mg^{2+}, Mn^{2+}, Ba^{2+}. As shown in Fig. 3b, the concentration of Pb^{2+} and other metal ions was 1 μM and 100 μM, respectively. The fluorescence of other competitive metal ions was comparable to the background fluorescence, while a large enhancement of fluorescence was observed from Pb^{2+}. The result indicated that even at relatively high concentration levels, the potentially interfering metal ions generated only minimal responses, verifying that this system had high selectivity. That was comparable with the original DNAzyme-based method for Pb^{2+} detection. These results indicated that the method had high sensitivity and good selectivity for the quantitative analysis of Pb^{2+}.

Pb^{2+} detection in real samples

To evaluate the application feasibility of the proposed strategy for Pb^{2+} detection in real samples, the recovery experiments are carried out by spiking Pb^{2+} into the environmental samples of tap water. The results are summarized in Table 2. Satisfactory recovery is found from 92.5 to 111.4%. Meanwhile, the results obtained by the prepared fluorescent strategy are consistent with the results of ICP-MS, indicating that the prepared method is suitable for Pb^{2+} detection in the real samples.

Intracellular detection

To explore the Pb^{2+} imaging capability in living cells, the DNAzyme@ZIF-8 composite was applied in 293 T cells and Huh-7 cells. As shown in Fig. 4, weak fluorescence was observed in the background fluorescence images, which was recorded after the incubation of DNAzyme@ZIF-8 and cells without Pb^{2+} for 4 h. After incubating with Pb^{2+}, partial fluorescence intensity increase was observed in 4 h, verifying the feasibility of the method in Pb^{2+} detection in living cells. Afterwards, significant fluorescence enhancement could be seen after incubating for 24 h. The concentration of Pb^{2+} was also determined 1.62 μg/L (311.2 nM in 293 cells) and 0.73 μg/L (140.4 nM in Huh-7 cells) by ICP-MS after cell digestion. Compared with other reported Pb^{2+} assay in cells [47, 48], it is found that the proposed method shows excellent analytical performances in situ cellular imaging. The results showed that the synthesized DNAzyme@ZIF-8 composite could easily penetrate 293 T cells and Huh-7 cells to detect Pb^{2+}, which further demonstrated the potential for metal ions detection in the living cells.

Conclusion

In summary, we have presented an efficiently biomimetic mineralization strategy to encapsulate GR-5 as model

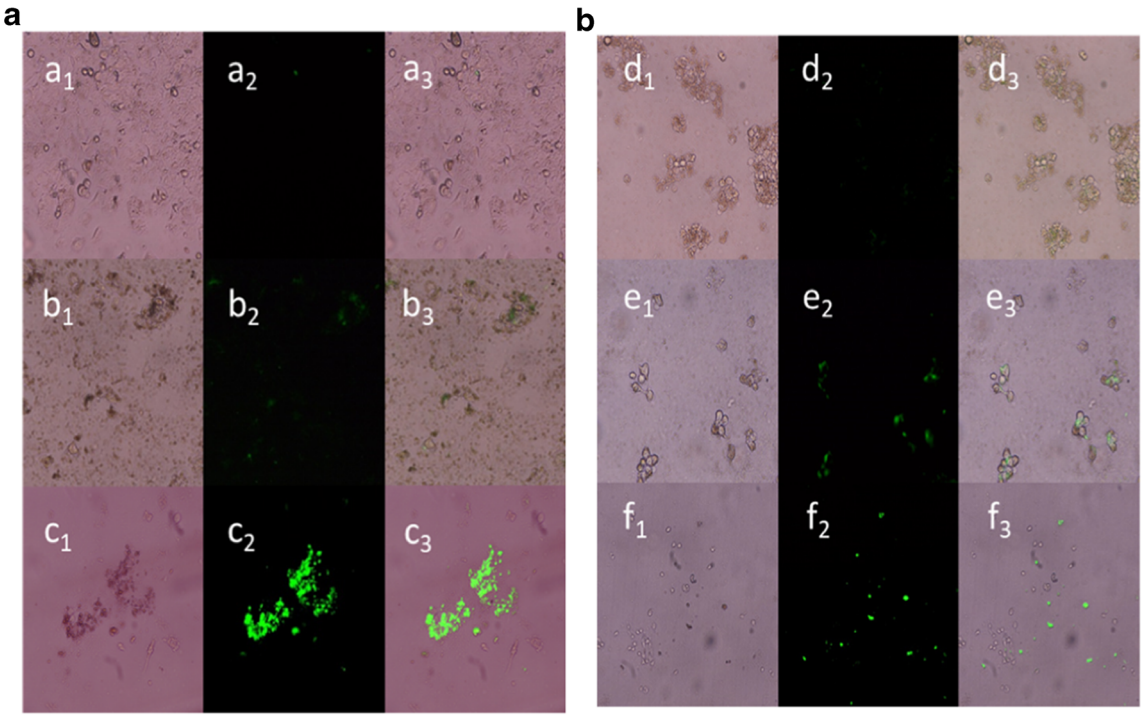

Fig. 4 **a** LSCM images of 293 T cells. Bright-field image (a_1–c_1); fluorescence image of the diverse incubation time (0, 4 h, 24 h) of DNAzyme@ZIF-8 and Pb^{2+} in 293 T cells(a_2–c_2); merge image (a_3–c_3). **b**) LSCM images of Huh-7 cells. Bright-field image (d_1–f_1); fluorescence image of the diverse incubation time (0, 4 h, 24 h) of DNAzyme@ZIF-8 and Pb^{2+} in Huh-7 cells(d_2–f_2); merge image (d_3–f_3)

DNAzyme into ZIF-8. The facile immobilization strategy could not only guarantee the intrinsic functions of DNAzyme but also effectively enhance the tolerance of DNAzyme towards proteolysis and cellular uptake efficiency of DNAzyme. Benefiting from the high DNAzyme loading capacity, the as-synthesized DNAzyme@ZIF-8 composite has realized the highly sensitive and selective fluorescent detection for Pb^{2+} in water and bioimaging of Pb^{2+} in living cells. We anticipate that this facile and versatile biomineralization strategy would fulfill the efficient protection and delivery of functional biomacromolecules, and further facilitate their application in such as industrial biocatalysis, biosensing, and bioimaging. Although the prepared DNAzyme@ZIF-8 composite has demonstrated impressive feasibility in detecting Pb^{2+} in water and cells, uncertain metal ions may interfere with the selectivity of this system, which would obstacle to expand the scope of its applications.

Author contributions Weihao Wu and Yaofang Fan contributed equally.

Funding This work was supported by the National Natural Science Foundation of China (No. 21976022).

Compliance with ethical standards

Conflict of interest The authors declare that they have no competing interests.

References

1. Breaker RR, Joyce GF (1994) A DNA enzyme that cleaves RNA. Chem Biol 1(4):223–229. https://doi.org/10.1016/1074-5521(94)90014-0
2. Zhang JJ (2018) RNA-cleaving DNAzymes: old catalysts with new tricks for intracellular and in vivo applications. Catalysts 8(11):550. https://doi.org/10.3390/catal8110550
3. Liu ZJ, Mei SHJ, Brennan JD, Li YF (2003) Assemblage of signaling DNA enzymes with intriguing metal-ion specificities and pH dependences. J Am Chem Soc 125(25):7539–7545. https://doi.org/10.1021/ja035208+
4. Mei SHJ, Liu ZJ, Brennan JD, Li YF (2003) An efficient RNA-cleaving DNA enzyme that synchronizes catalysis with fluorescence signaling. J Am Chem Soc 125(2):412–420. https://doi.org/10.1021/ja0281232
5. Sidorov AV, Grasby JA, Williams DM (2004) Sequence-specific cleavage of RNA in the absence of divalent metal ions by a DNAzyme incorporating imidazolyl and amino functionalities. Nucleic Acids Res 32(4):1591–1601. https://doi.org/10.1093/nar/gkh326
6. Liu JW, Brown AK, Meng XL, Cropek DM, Istok JD, Watson DB, Lu Y (2007) A catalytic beacon sensor for uranium with parts-per-trillion sensitivity and millionfold selectivity. PNAS 104(7):2056–2061. https://doi.org/10.1073/pnas.0607875104
7. Carmi N, Shultz LA, Breaker RR (1996) In vitro selection of self-cleaving DNAs. Chem Biol 3(12):1039–1046. https://doi.org/10.1016/S1074-5521(96)90170-2
8. Carmi N, Balkhi SR, Breaker RR (1998) Cleaving DNA with DNA. PNAS 95(5):2233–2237. https://doi.org/10.1073/pnas.95.5.2233
9. Purtha WE, Coppins RL, Smalley MK, Silverman SK (2005) General deoxyribozyme-catalyzed synthesis of native 3 '-5 ' RNA linkages. J Am Chem Soc 127(38):13124–13125. https://doi.org/10.1021/ja0533702
10. Hoadley KA, Purtha WE, Wolf AC, Flynn-Charlebois A, Silverman SK (2005) Zn^{2+}-dependent deoxyribozymes that form natural and unnatural RNA linkages. Biochemistry 44(25):9217–9231. https://doi.org/10.1021/bi050146g
11. Sreedhara A, Li YF, Breaker RR (2004) Ligating DNA with DNA. J Am Chem Soc 126(11):3454–3460. https://doi.org/10.1021/ja039713i
12. Wang W, Billen LP, Li YF (2002) Sequence diversity, metal specificity, and catalytic proficiency of metal-dependent phosphorylating DNA enzymes. Chem Biol 9(4):507–517. https://doi.org/10.1016/S1074-5521(02)00127-8
13. Wang W, Satyavolu NSR, Wu Z, Zhang JR, Zhu JJ, Lu Y (2017) Near-infrared photothermally activated DNAzyme-gold nanoshells for imaging metal ions in living cells. Angew Chem Int Ed Eng 56(24):6798–6802. https://doi.org/10.1002/anie.201701325
14. McGhee CE, Loh KY, Lu Y (2017) DNAzyme sensors for detection of metal ions in the environment and imaging them in living cells. Curr Opin Biotechnol 45:191–201. https://doi.org/10.1016/j.copbio.2017.03.002
15. Zhang XB, Kong RM, Lu Y (2011) Metal ion sensors based on DNAzymes and related DNA molecules. Annu Rev Anal Chem (Palo Alto, Calif) 4:105–128. https://doi.org/10.1146/annurev.anchem.111808.073617
16. Meng LX, Liu MY, Xiao K, Zhang XH, Du CC, Chen JH (2020) Sensitive photoelectrochemical assay of $Pb^{(2+)}$ based on DNAzyme-induced disassembly of the "Z-Scheme" TiO_2/Au/CdS QDs system. Chem Commun (Camb) 56:8261–8264. https://doi.org/10.1039/d0cc03149f
17. Wu Z, Fan H, Satyavolu NSR, Wang W, Lake R, Jiang JH, Lu Y (2017) Imaging endogenous metal ions in living cells using a DNAzyme-catalytic hairpin assembly probe. Angew Chem Int Ed Eng 56(30):8721–8725. https://doi.org/10.1002/anie.201703540
18. Wang HM, Chen YQ, Wang H, Liu XQ, Zhou X, Wang F (2019) DNAzyme-loaded metal-organic frameworks (MOFs) for self-sufficient gene therapy. Angew Chem Int Ed Eng 58(22):7380–7384. https://doi.org/10.1002/anie.201902714
19. Zhang C, Zhang L, Wu W, Gao F, Li RQ, Song W, Zhuang ZN, Liu CJ, Zhang XZ (2019) Artificial super neutrophils for inflammation targeting and HClO generation against tumors and infections. Adv Mater 31(19):e1901179. https://doi.org/10.1002/adma.201901179
20. Liang W, Carraro F, Solomon MB, Bell SG, Amenitsch H, Sumby CJ, White NG, Falcaro P, Doonan CJ (2019) Enzyme encapsulation in a porous hydrogen-bonded organic framework. J Am Chem Soc 141(36):14298–14305. https://doi.org/10.1021/jacs.9b06589
21. Ouyang G; Chen G; Huang S; Kou X; Wei S; Huang S; Jiang S; Shen J; Zhu F (2018) A convenient and versatile amino acid-boosted biomimetic strategy for nondestructive encapsulation of biomacromolecules within metal-organic framework. Angew Chem (International ed. in English)
22. Gimenez-Marques M, Hidalgo T, Serre C, Horcajada P (2016) Nanostructured metal-organic frameworks and their bio-related applications. Coord Chem Rev 307:342–360. https://doi.org/10.1016/j.ccr.2015.08.008
23. Liang K, Ricco R, Doherty CM, Styles MJ, Bell S, Kirby N, Mudie S, Haylock D, Hill AJ, Doonan CJ, Falcaro P (2015) Biomimetic mineralization of metal-organic frameworks as protective coatings for biomacromolecules. Nat Commun 6:7240. https://doi.org/10.1038/ncomms8240

24. Qin FX, Jia SY, Wang FF, Wu SH, Song J, Liu Y (2013) Hemin@metal-organic framework with peroxidase-like activity and its application to glucose detection. Catal Sci Technol 3(10): 2761–2768. https://doi.org/10.1039/C3CY00268C
25. Cui L, Wu J, Li J, Ju H (2015) Electrochemical sensor for lead cation sensitized with a DNA functionalized porphyrinic metal-organic framework. Anal Chem 87(20):10635–10641. https://doi.org/10.1021/acs.analchem.5b03287
26. Pisklak TJ, Macias M, Coutinho DH, Huang RS, Balkus KJ (2006) Hybrid materials for immobilization of MP-11 catalyst. Top Catal 38(4):269–278. https://doi.org/10.1007/s11244-006-0025-6
27. Mehta J, Bhardwaj N, Bhardwaj SK, Kim KH, Deep A (2016) Recent advances in enzyme immobilization techniques: metal-organic frameworks as novel substrates. Coord Chem Rev 322: 30–40. https://doi.org/10.1016/j.ccr.2016.05.007
28. Gkaniatsou E, Sicard C, Ricoux R, Mahy JP, Steunou N, Serre C (2017) Metal-organic frameworks: a novel host platform for enzymatic catalysis and detection. Mater Horiz 4(1):55–63. https://doi.org/10.1039/c6mh00312e
29. Shao C, Liang J, He SH, Luan TQ, Yu JT, Zhao HR, Xu JY, Tian LL (2017) pH-responsive graphene oxide-DNA nanosystem for live cell imaging and detection. Anal Chem 89(10):5445–5452. https://doi.org/10.1021/acs.analchem.7b00369
30. Horcajada P, Chalati T, Serre C, Gillet B, Sebrie C, Baati T, Eubank JF, Heurtaux D, Clayette P, Kreuz C, Chang JS, Hwang YK, Marsaud V, Bories PN, Cynober L, Gil S, Ferey G, Couvreur P, Gref R (2010) Porous metal-organic-framework nanoscale carriers as a potential platform for drug delivery and imaging. Nat Mater 9(2):172–178. https://doi.org/10.1038/NMAT2608
31. Phan A, Doonan CJ, Uribe-Romo FJ, Knobler CB, O'Keeffe M, Yaghi OM (2010) Synthesis, structure, and carbon dioxide capture properties of zeolitic imidazolate frameworks. Acc Chem Res 43(1):58–67. https://doi.org/10.1021/ar900116g
32. Alsaiari SK, Patil S, Alyami M, Alamoudi KO, Aleisa FA, Merzaban JS, Li M, Khashab NM (2018) Endosomal escape and delivery of CRISPR/Cas9 genome editing machinery enabled by nanoscale zeolitic imidazolate framework. J Am Chem Soc 140(1): 143–146. https://doi.org/10.1021/jacs.7b11754
33. Wu X, Ge J, Yang C, Hou M, Liu Z (2015) Facile synthesis of multiple enzyme-containing metal-organic frameworks in a biomolecule-friendly environment. Chem Commun 51(69): 13408–13411. https://doi.org/10.1039/c5cc05136c
34. Guo Y, Jiang ZQ, Ying W, Chen LP, Liu YZ, Wang XB, Jiang ZJ, Chen BL, Peng XS (2018) A DNA-threaded ZIF-8 membrane with high proton conductivity and low methanol permeability. Adv Mater 30(2). https://doi.org/10.1002/adma.201705155
35. Torchilin V (2011) Tumor delivery of macromolecular drugs based on the EPR effect. Adv Drug Deliv Rev 63(3):131–135. https://doi.org/10.1016/j.addr.2010.03.011
36. Davis ME, Chen ZG, Shin DM (2008) Nanoparticle therapeutics: an emerging treatment modality for cancer. Nat Rev Drug Discov 7(9):771–782. https://doi.org/10.1038/nrd2614
37. Poddar A, Conesa JJ, Liang K, Dhakal S, Reineck P, Bryant G, Pereiro E, Ricco R, Amenitsch H, Doonan C, Mulet X, Doherty CM, Falcaro P, Shukla R (2019) Encapsulation, visualization and expression of genes with biomimetically mineralized zeolitic imidazolate framework-8 (ZIF-8). Small 15(36):1902268. https://doi.org/10.1002/smll.201902268
38. Yang XT, Tang Q, Jiang Y, Zhang MN, Wang M, Mao LQ (2019) Nanoscale ATP-responsive zeolitic imidazole framework-90 as a general platform for cytosolic protein delivery and genome editing. J Am Chem Soc 141(9):3782–3786. https://doi.org/10.1021/jacs.8b11996
39. Yi JT, Chen TT, Huo J, Chu X (2017) Nanoscale zeolitic imidazolate framework-8 for ratiometric fluorescence imaging of MicroRNA in living cells. Anal Chem 89(22):12351–12359. https://doi.org/10.1021/acs.analchem.7b03369
40. Chen BL, Yang ZX, Zhu YQ, Xia YD (2014) Zeolitic imidazolate framework materials: recent progress in synthesis and applications. J Mater Chem A 2(40):16811–16831. https://doi.org/10.1039/c4ta02984d
41. Lan T, Furuya K, Lu YA (2010) Highly selective lead sensor based on a classic lead DNAzyme. Chem Commun 46(22):3896–3898. https://doi.org/10.1039/b926910j
42. Zhao XH, Kong RM, Zhang XB, Meng HM, Liu WN, Tan WH, Shen GL, Yu RQ (2011) Graphene-DNAzyme based biosensor for amplified fluorescence "turn-on" detection of Pb^{2+} with a high selectivity. Anal Chem 83(13):5062–5066. https://doi.org/10.1021/ac200843x
43. Wang RY, Zhou XH, Shi HC (2015) Triple functional DNA-protein conjugates: signal probes for Pb^{2+} using evanescent wave-induced emission. Biosens Bioelectron 74:78–84. https://doi.org/10.1016/j.bios.2015.06.003
44. Memon AG, Zhou XH, Xing YP, Wang RY, Liu LH, Khan M, He M (2019) Label-free colorimetric nanosensor with improved sensitivity for Pb^{2+} in water by using a truncated 8–17 DNAzyme. Front Environ Sci Eng 13(1). https://doi.org/10.1007/s11783-019-1094-7
45. Guo Y, Li JT, Zhang XQ, Tang YL (2015) A sensitive biosensor with a DNAzyme for lead(ii) detection based on fluorescence turn-on. Analyst 140(13):4642–4647. https://doi.org/10.1039/c5an00677e
46. Wang J, Zhang Z, Gao X, Lin X, Liu Y, Wang S (2019) A single fluorophore ratiometric nanosensor based on dual-emission DNA-templated silver nanoclusters for ultrasensitive and selective Pb^{2+} detection. Sensors Actuators B Chem 282:712–718. https://doi.org/10.1016/j.snb.2018.11.121
47. Sannigrahi A, Chowdhury S, Nandi I, Sanyal D, Chall S, Chattopadhyay K (2019) Development of a near infrared Au–Ag bimetallic nanocluster for ultrasensitive detection of toxic Pb^{2+} ions in vitro and inside cells. Nanoscale Adv 1(9):3660–3669. https://doi.org/10.1039/c9na00459a
48. Cui MR, Li XL, Xu JJ, Chen HY (2020) Acid-switchable DNAzyme nanodevice for imaging multiple metal ions in living cells. ACS Appl Mater Interfaces 12(11):13005–13012. https://doi.org/10.1021/acsami.0c00987